

Article

# Characteristic Analysis and Predictive Torque Control of the Modular Three-Phase PMSM for Low-Voltage High Power Application

Zhimeng Rao <sup>1</sup>, Wenjuan Zhang <sup>2,\*</sup>, Gongping Wu <sup>1</sup>, Jian Zheng <sup>3</sup> and Shoudao Huang <sup>1</sup>

<sup>1</sup> College of Electrical and Information Engineering, Hunan University, Changsha 410082, China; zhimeng\_rao@hnu.edu.cn (Z.R.); gongping\_wu@hnu.edu.cn (G.W.); shoudao\_huang@hnu.edu.cn (S.H.)

<sup>2</sup> College of Electrical and Information Engineering, Changsha University, Changsha 410082, China

<sup>3</sup> College of Electrical and Information Engineering, Hunan University of Technology, Zhuzhou 412007, China; zj11660@hut.edu.cn

\* Correspondence: z20141074@ccsu.edu.cn; Tel.: +86-186-9220-8506

Received: 27 August 2020; Accepted: 22 October 2020; Published: 27 October 2020



**Abstract:** In this study, a novel modular three-phase permanent magnet synchronous motor (PMSM) is proposed for low-voltage high power applications. The proposed modular three-phase PMSM has an independent segregated three-phase winding configuration, facilitating the implementation of the control algorithm. Firstly, on the basis of the electromagnetic properties, the mathematical model of the modular three-phase PMSM is established, considering the asymmetrical mutual inductances investigated by finite element analysis (FEA). Then, the predictive torque control (PTC) method combining the inductance characteristics of modular three-phase PMSM is developed, and excellent performance is obtained by adjusting the stator flux and torque. Finally, simulation and experiment are performed, and the results show that the proposed novel modular three-phase PMSM with the PTC method exhibits excellent control performance, and small stator current total harmonic distortion (THD).

**Keywords:** modular three-phase permanent magnet synchronous motor (PMSM), finite element analysis; predictive torque control; mutual inductances

## 1. Introduction

The permanent magnet synchronous motor (PMSM) has been paid more and more attention in industrial applications owing to advantages such as high power/torque density, high efficiency, and its flux-weakening property [1,2]. With the increase of power level, a three-phase PMSM based on a single voltage source inverter (VSI) cannot supply power for high-power traction applications [3]. To meet the requirements of higher power traction, the most straightforward method proposed is to employ a multi-converter system structure either in series or in parallel [4,5]. However, the three-phase winding currents of PMSM fed by multi-converters are still too high to generate the rated power.

In general, the multi-three-phase PMSM increases the number of phases by keeping the input voltage and output power the same, which can dramatically decrease the current stress level in power devices [6–8]. Therefore, the multi-three-phase PMSM has been considered a feasible alternative for low-voltage large power applications, and has attracted more and more attention in recent years. The implementation of the multi-three-phase PMSM control strategy usually depends on the multiple d-q modeling method or the vector space decomposition modeling method [9–11]. Because the stator windings of the multi-three-phase PMSM are overlapped, cross-coupled fields are formed among the multiple winding sets. Therefore, no matter which modeling approach is employed, a customized controller is needed, which will lead to a significant increase in cost and design time.

To facilitate the implementation of the control algorithm of the multi-three-phase PMSM, the modular three-phase PMSM with a novel and untraditional stator winding arrangement has attracted the attention of scholars [12–21]. The merit of the stator winding placement is that the mutual couplings among the multi-three-phase winding sets are negligible. Each winding set can be fed by a conventional three-phase VSI, as depicted in Figure 1. In [12–15], a novel PMSM with different winding configurations and displacements were studied, offering a good alternative for high-power traction application owing to higher average torque and lower torque ripple. In [19], a general modeling method for a triple three-phase permanent magnet assisted synchronous reluctance machine with segregated winding sets was proposed, offering excellent flexibility for fault monitoring performance evaluation, fault detection, and post fault control. In [20], a multi-segment PMSM drive system with phase-shift pulse width modulation (PWM) was presented, which can meet the requirements of lower torque ripple, vibration, and noise. Furthermore, the circulating current between the two VSIs can be avoided with this winding configuration. In [21], a dual three-phase PMSM topology fed by two T-type neutral point clamped inverters was proposed for low-voltage and high-power applications, realizing the decoupling of PWM control and dc-link capacitor voltage balance control.

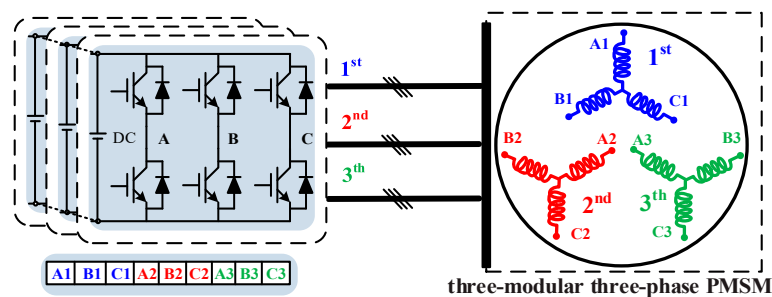


**Figure 1.** Drive topology of the modular three-phase permanent magnet synchronous motor (PMSM) structure.

In [12–21], the asymmetrical mutual inductances of each motor unit caused by the segregated winding configuration are not considered when the mathematical model of modular three-phase PMSM is established, which can dramatically affect the static and dynamic characteristics. In addition, the modular three-phase PMSM in the actual operation process is a nonlinear system with parameter variation and uncertain disturbance. However, the parameter settings of the proportional-integral (PI) controllers only correspond to some specific working range. Thus, this causes problems with controllers when the working state of the motor changes [22]. It is difficult to gain a better dynamic control performance using field-oriented control (FOC) with independent regulation of d-q axis currents with PI controllers in the whole operating range. The predictive torque control (PTC) becomes more and more attractive in the PMSM control due to its excellent transient response characteristics and accurate reference current tracking [23,24].

Therefore, in this paper, a novel modular three-phase PMSM with the PTC method concerning the asymmetrical mutual inductances is proposed. The main contributions of this paper are threefold:

1. Compared with the traditional multiphase machine, the modular three-phase PMSM with the unconventional stator winding placement has the advantages of simpler structure, low cost, and facilitating the control method implementation.
2. The mathematical model considering the asymmetrical mutual inductances of the modular three-phase PMSM is established to provide a more accurate torque control.
3. The simulation results show that the torque ripple is lower than that achieved with the PI method and the experimental results show that the proposed machine with the PTC method can obtain a small stator current total harmonic distortion (THD).

This paper is organized as follows: the characteristic analysis of the modular three-phase PMSM is described in Section 2. The mathematical model of the proposed machine, considering the asymmetrical

mutual inductances, is presented in Section 3. The PTC control of the modular three-phase PMSM is analyzed in Section 4. In Section 5, the prototype motor is manufactured and tested to verify the validity of the proposed PTC and motors. Finally, conclusions are drawn in Section 6.

## 2. The Characteristic Analysis of the Modular Three-Phase PMSM

### 2.1. Topology Winding Configuration of the Modular Three-Phase PMSM

The proposed modular machine with an unconventional winding placement consists of  $N$  sets of segregated motor units ( $A_i B_i C_i$ , where  $i = 1, 2 \dots N$ ), sharing one set of the permanent magnet (PM) rotor. Each motor unit has the same electromagnetic characteristics, and thus the total power and torque are evenly divided by the  $N$  sets of motor units. Taking the triple module three-phase PMSM and symmetrical 9-phase PMSM as an example, the structure diagrams are given in Figure 2, and the winding alternatives and phasor diagrams are depicted in Figure 3. In the case of the symmetrical 9-phase PMSM, the distributed windings of different sets are overlapped and contacted together, as shown in Figure 2a or Figure 3a. As a result, a strong cross-coupling magnetic field needing full-coupling compensation would exist among three-phase winding sets. Alternatively, the traditional overlapped windings are wound into three discrete segments along the circumference of the stator core without any penalties or additional cost, so there is no physical contact among winding sets, as depicted in Figure 2b or Figure 3b.

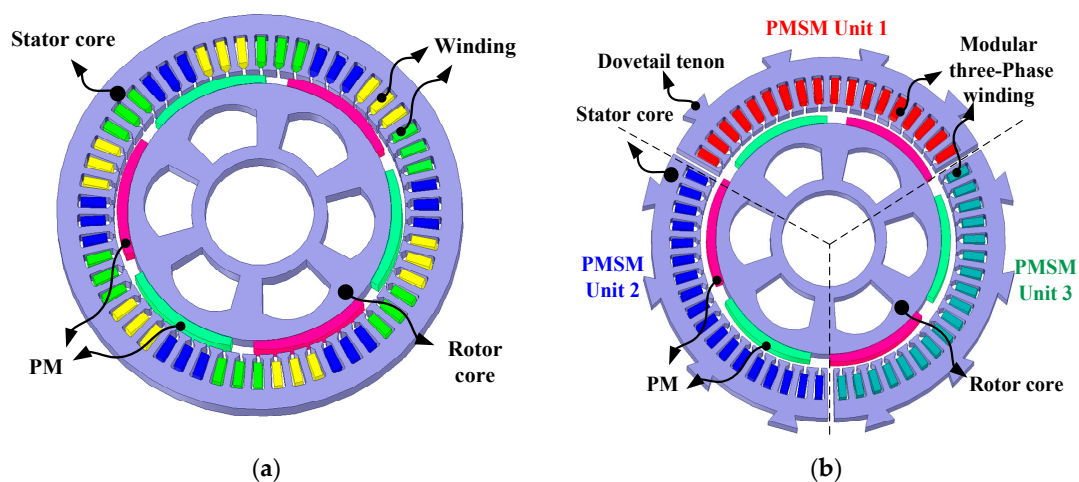


Figure 2. Structure diagrams: (a) symmetrical 9-phase PMSM, (b) modular three-phase PMSM.

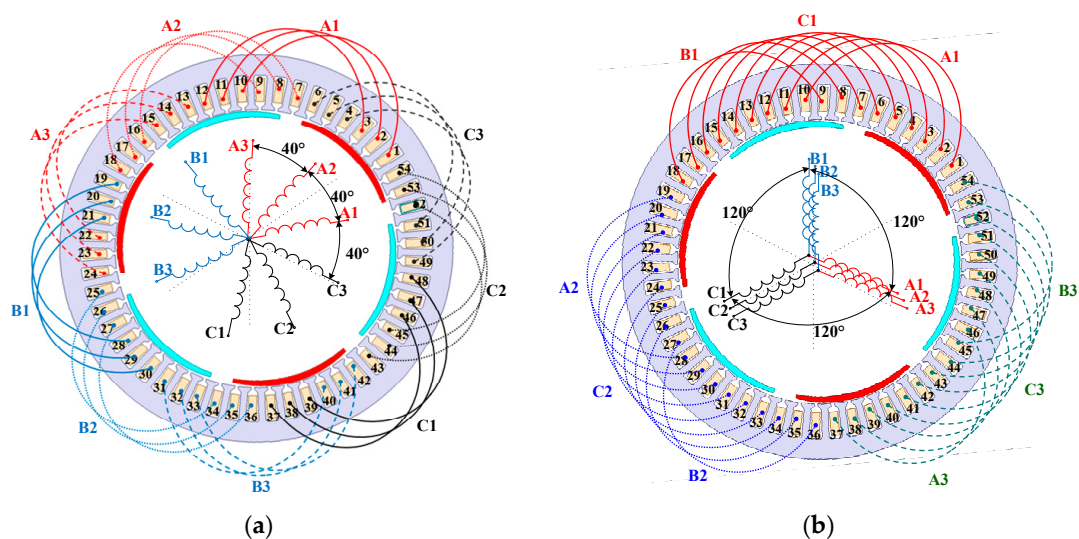


Figure 3. Structure diagrams: (a) symmetrical 9-phase PMSM, (b) modular three-phase PMSM.

As stated in [12–21], if the three-phase winding of the motor unit does not share any slot with the other motor units, the mutual inductances among the three motor units can be negligible, realizing independent control of each winding set and dramatically reducing the difficulty of controller design. The neutral points of different three-phase winding sets are isolated from each other. Thus, each isolated three-phase winding set can be driven by a well-consolidated two-level VSI, which is prone to facilitate extremely fast integration and cost reduction. In the event of a fault in one part of the stator winding sets, the faulty winding could be cut off and isolated from VSI by the controller owing to the configuration of the separated windings. In addition, the other healthy winding sets are capable of uninterrupted operation to deliver torque or power without any sophisticated control algorithm.

## 2.2. Finite Element Analysis (FEA) of Modular Three-Phase PMSM

In this section, a triple module three-phase PMSM model with a 54-slot, 6-pole combination, and surface-mounted PM rotor is established. The main unit motor parameters are given in Table 1, featured by a single-layer winding with the segregated coils. The Ansys/Maxwell package software was used to obtain the results presented in the paper.

Table 1. Main Parameters of Unit Motor.

Parameter	Value	Parameter	Value
Rated power	53 kW	Rotor flux	0.799 Wb
Rated speed	800 r/min	Stator resistance	0.02 $\Omega$
Rated current	130 A	d axis inductance	2.5 mH
Stator outer diameter	600 mm	q axis inductance	4.1 mH
Stator stack length	1500 mm	Type of magnet	$B_r = 1.2$ T, $u_r = 1.05$

The two figures in Figure 4 are in a no-load condition. The figure on the left shows the magnetic density of the machine. As can be seen from the figure, no saturation can be observed, and the stator tooth has the maximum magnetic density (1.42 T), which is suitable for most working conditions. The figure on the right shows the distribution of magnetic force lines of the machine. It can be seen that the magnetic line distribution repeats three times along the stator circumference.

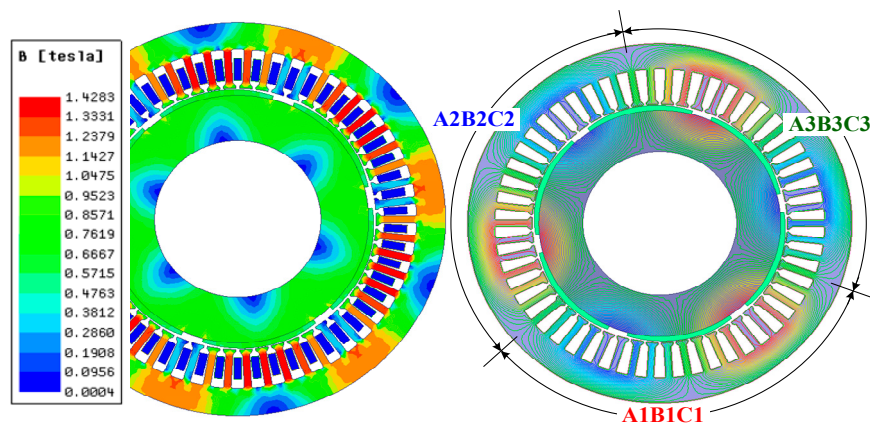


Figure 4. Flux contour.

The no-load back electromotive force waveform of the triple module three-phase PMSM at 800 r/min is depicted in Figure 5. The phase shifts among multiple winding sets can be distinctly seen from the FEA analytical results. In the triple module three-phase PMSM, the angle differences among  $A_i$ ,  $B_i$ , and  $C_i$  ( $i = 1,2,3$ ) are 120 electrical degrees, the angle differences among  $A_i$  ( $i = 1,2,3$ ) are 0 electrical degrees, which is entirely in agreement with the analysis of Figure 3b. The amplitude of the no-load back electromotive force voltage of each motor unit is almost the same (185 V) with lower harmonic content (5.1%).

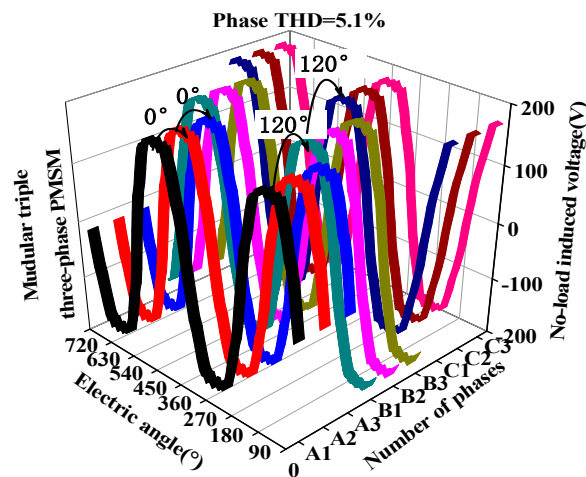


Figure 5. Back electromotive force waveform.

The on-load analysis of the proposed triple module three-phase PMSM is also investigated. As seen in Figure 6, the output torque of each motor unit is the same. In addition, the output torques of motor units 1 and 2 are equal to that of the motor units 1 and 3, and all of them are twice the output torque of motor unit 1. The total output torque generated by the modular three-phase PMSM is the sum of each motor unit. In other words, each motor unit of the triple module three-phase PMSM has a good independence and superposition characteristic. In addition, the torque ripple factor is defined as the ratio of peak-to-peak torque value to average torque value. The torque ripple factors of unit motor and triple module three-phase PMSM are 13.4% and 6.3%.

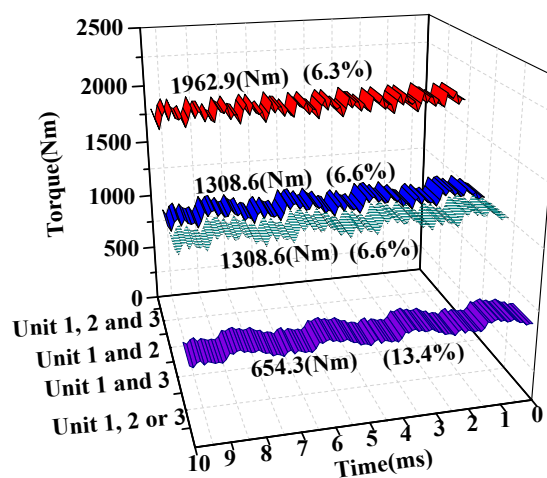


Figure 6. Output torque variation.

Figure 7 represents the flux lines distribution of the triple module three-phase PMSM when phase A1 is supplied by 100 A, and A2 and A3 are under no-load condition. As can be seen in Figure 7, there is weak cross-coupling flux among the phases A1, A2, and A3, respectively. The FEA results show that the self-inductance of the phase A1 is 5.1 mH, and the mutual-inductance of the phases A1 and A2 is the same as that of A1 and A3 (0.25 mH), only 4.9% of self-inductance. It means that with this configuration, the cross-coupling effects among triple three-phase winding sets are negligible and significantly less than that of the self-inductance of each phase winding. The winding sets of the three-segment motors fed independently are merely combined in the electromagnetic torque, which is the foundation of the control strategy.

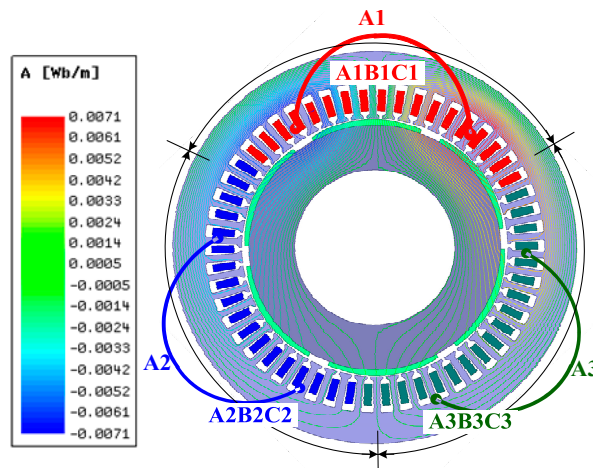


Figure 7. Armature reaction of phase A1.

### 2.3. Winding Inductance Characteristics of Modular Three-Phase PMSM

The inductances are basic parameters for the modular three-phase PMSM, dramatically affecting the dynamic behavior and performance. In addition, the accuracy of the mathematical model of inductance is crucial for the PTC control strategy. Hence, the more accurate incremental inductance method based on the FEA is used to investigate the inductance characteristics of the proposed modular three-phase PMSM.

The flux linkage produced by the unit current can be calculated by subtracting the PM flux linkage from the flux linkage generated by the unit current of the coil 1 and the PM flux linkage, as exhibited in Figure 8. According to the definition of incremental inductance, the self-inductance of the coil 1 can be calculated by dividing the flux arising from the unit current by the winding current. The specific calculation formula in an abc three-phase stationary coordinate system can be written as follows

$$\begin{cases} L_{11} = \frac{\psi_1 - \psi_0}{I} \\ M_{21} = \frac{\psi_2 - \psi_0}{I} \end{cases} \quad (1)$$

where  $L_{11}$  is the self-inductance of the coil 1,  $\psi_0$  is the flux linkage of coil 1 produced by PM,  $I$  is the unit current,  $\psi_1$  is the flux linkage of coil 1 arising from the unit current and PM,  $\psi_2$  is the flux linkage of coil 2, and  $M_{21}$  is the mutual inductance between coil 1 and coil 2. Obviously, the self-inductance of coil 1 depends not only on the current level but also on the rotor position, which is influenced by the saturation effect due to magnets and armature currents. Under the condition of zero current, the permeability of the stator core changes linearly. The permeability of the stator core changes linearly, and the inductance value is almost constant. When a small current is applied to coil 1, the inductance can be calculated according to Equation (1). The inductance value can be approximate to that at 0 current moment.

Eventually, by applying (1) to the armature reaction flux linkage, the self-inductance and mutual inductance of phase A1 can be acquired. The self-inductances and mutual inductances of the triple module three-phase PMSM generated by the phase A1 ( $I_{max} = 100$  A) can be obtained, as illustrated in Figure 9. The self-inductance of phase A1 is most significant, followed by the mutual inductances  $L_{A1C1}$  and  $L_{A1B1}$ . Although phase B3 is also adjacent to phase A1, it belongs to the different motor units. As stated in [19], the magnetic couplings among three winding sets become very low (0.4 mH), which can be negligible.

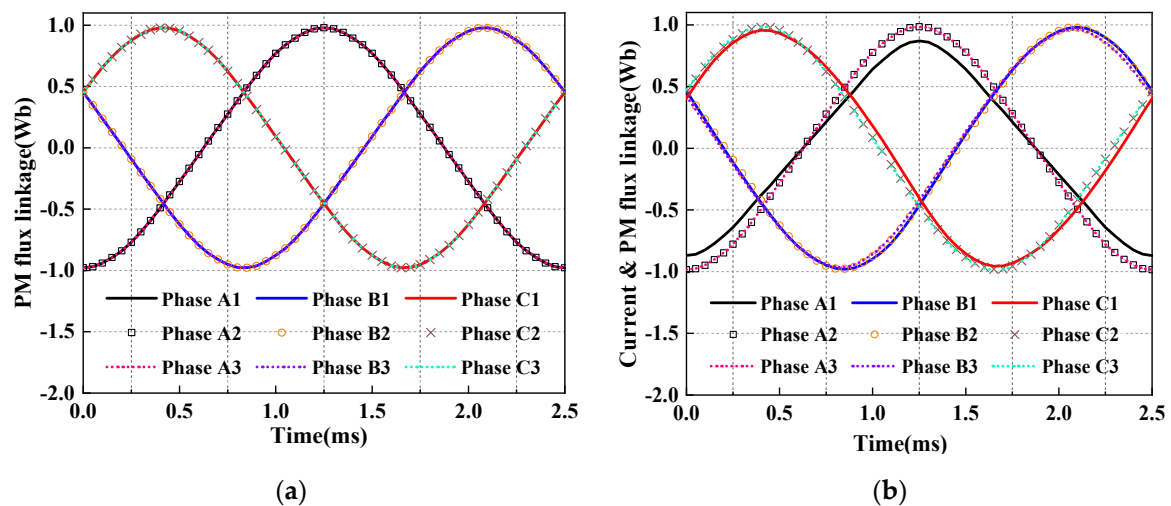


Figure 8. Flux linkage: (a) permanent magnet (PM) flux linkage, (b) combined flux linkage (A1 current  $I_{max} = 100$  A).

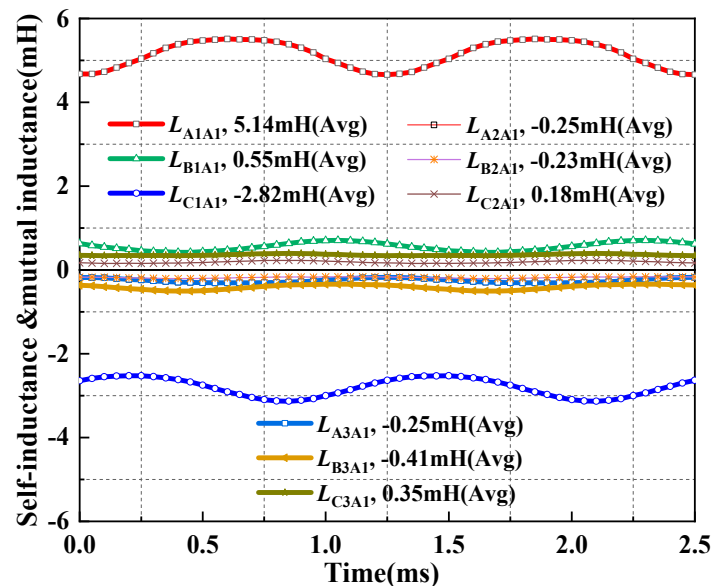


Figure 9. Self and mutual inductance of phase A1.

The inductance characteristics of motor unit 1 are depicted in Figure 10. As shown in Figure 10, both the self-inductances and mutual inductances are quite sinusoidal with twice the frequency of the flux linkage. The amplitudes of the self-inductances of the three-phase winding set of motor unit 1 are the same with an angle difference of 60 electrical degrees, which is identical to conventional three-phase PMSM. Meanwhile, the amplitudes of the mutual inductance  $L_{C1A1}$  and  $L_{B1C1}$  are 2.8 mH and  $L_{B1A1}$  is 0.55 mH. It is remarkable that the average values of the mutual inductances  $L_{C1A1}$  and  $L_{B1C1}$  are much bigger than that of the mutual inductance  $L_{B1A1}$ , which is somewhat different from the conventional three-phase PMSM. The reason is that each motor unit only occupies one sector of the whole stator core, and the three-phase winding set is evenly distributed along the stator core circumference. The three-phase windings are asymmetrical in spatial position. Thus, the spatial angle difference of phases A1 and C1 is equal to that of phases B1 and C1, and is half of phases A1 and B1, which will inevitably lead to inconsistent mutual inductances of three-phase windings in each motor unit.

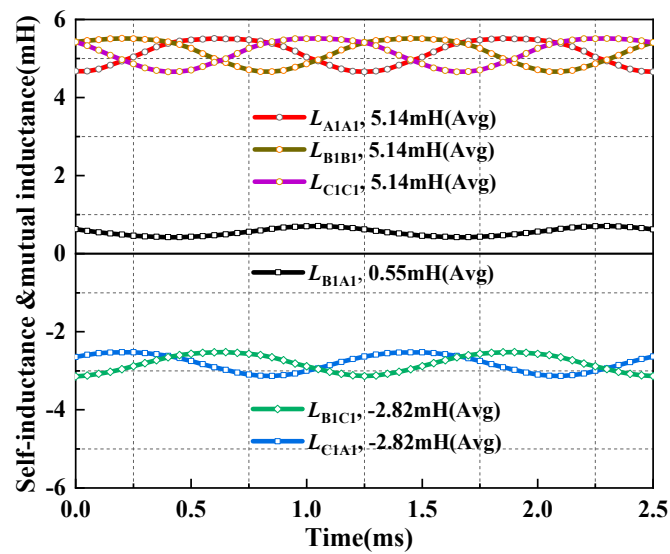


Figure 10. Inductance of motor unit 1.

Besides, the inductance characteristics of motor unit 1 versus the current ( $I_{max}$ ) of phase A1 are shown in Figure 11. The unsaturated self-inductance  $L_{A1A1}$  increases for the overall trend as phase A1 current increases from 0 to 200 A, though it changes nonlinearly. Nevertheless, the magnetic circuits of the proposed machine become oversaturated with a further increase of the current, resulting in a significant decrease in  $L_{A1A1}$ . From the Figure 11, it can be known that both  $L_{C1A1}$  and  $L_{B1C1}$  of motor unit 1 vary little with the increased current amplitude. The mutual inductance  $L_{B1A1}$  is less sensitive to the current compared with  $L_{C1A1}$  and  $L_{B1C1}$ , since the mutual inductances  $L_{B1A1}$  keeps almost unchanged.

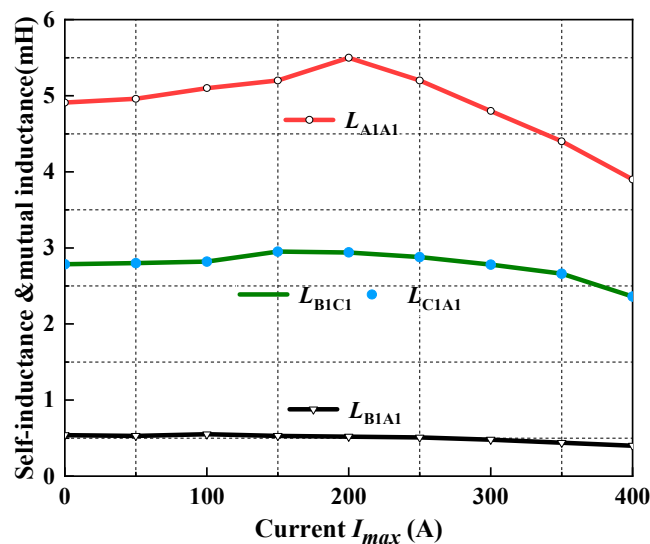


Figure 11. Inductances of motor 1 versus the current  $I_{max}$ .

In order to quantitatively study the inductance characteristics of the triple module three-phase PMSM, the fast Fourier transformation analysis of  $L_{A1A1}$ ,  $L_{A1C1}$ ,  $L_{B1C1}$ , and  $L_{A1B1}$  is employed and depicted in Figure 12. As can be seen, the 2nd harmonic is most abundant, followed by the 4th harmonic. Compared with the 2nd harmonic component, the 4th harmonic and other higher harmonics can be ignored. The critical values, such as the dc components and the 2nd harmonics magnitudes, are given in Table 2. It shows that the dc component of  $L_{A1B1}$  is considerably lower than  $L_{A1C1}$  and  $L_{B1C1}$ , which is much different from the conventional three-phase PMSM.

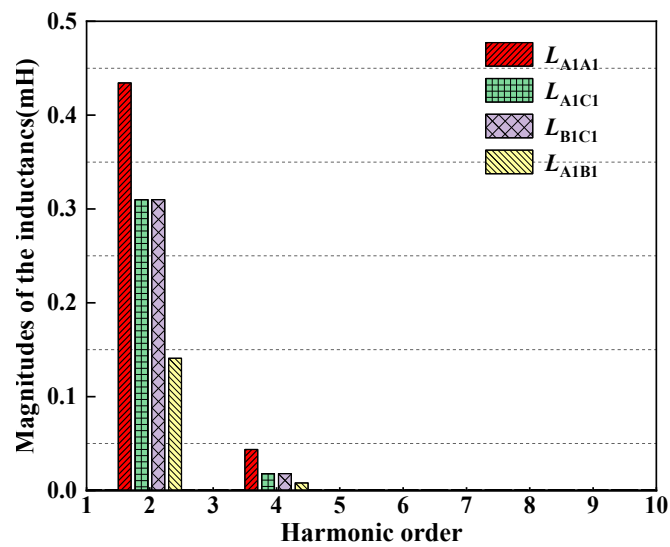


Figure 12. Harmonics distributions.

Table 2. Inductance Characteristics of Phase 1.

Parameter	Dc Component	The 2nd Harmonic (Peak)
$L_{A1A1}$	5.14 mH	0.43 mH
$L_{A1C1}$	2.81 mH	0.31 mH
$L_{B1C1}$	2.81 mH	0.31 mH
$L_{A1B1}$	0.55 mH	0.14 mH

Similarly, the influence caused by the inconsistent mutual inductances of each unit motor on the d-q axis inductances  $L_d$  and  $L_q$  is also analyzed. In general, the  $L_d$  and  $L_q$  of the motor unit can be calculated as follows

$$L(d, q, 0) = P * L(a, b, c) * P^{-1} \quad (2)$$

where  $P$  is the well-known Park-transformation matrix.

According to (2), the inductance characteristics of the d-axis and q-axis over one electrical cycle are shown in Figure 13. The fluctuation frequencies of the  $L_d$  and  $L_q$  are equal to that of the self-inductances. The average values of the  $L_d$  and  $L_q$  are 2.5 mH and 4.1 mH, respectively. It can be known that the average value of  $L_q$  is higher than that of  $L_d$ , even if the rotor adopts the surface-mounted PM structure. In this case, the salient effect will exist in each motor unit with the proposed winding configuration caused by the inconsistent mutual inductances. This feature is distinctive and unavoidable for the proposed machine, which should be considered in establishing accurate mathematical modeling for the modular three-phase PMSM. In addition, different from the three-phase and multi-phase PMSMs, the inductance difference value between  $L_q$  and  $L_d$  (i.e.,  $L_q - L_d$ ) varies sinusoidally. This phenomenon results in the periodic change of reluctance torque, which is not conducive to reducing torque ripple, which is needed to optimize motor design and improve control strategy.

Figure 14 depicts that the d-q axis inductances of motor unit 1 with different phase current conditions varied from 0 to 400 A. Additionally, the inductance difference between  $L_q$  and  $L_d$  is also investigated. As can be seen, the inductance  $L_d$  increases then turn to decrease with the increased current amplitude, but the inductance  $L_q$  decreases gradually as the current increases.  $L_q - L_d$  is a positive value as the phase current below 263 A and then is negative with the further growth of the phase current, which is much different from conventional three-phase PMSM. It means that the modular three-phase PMSM can run with a positive d-axis current ( $i_d$ ), which is beneficial to realize the flux-intensifying effect and reduce the demagnetization risk of the module three-phase PMSM under the high current amplitude condition or the condition that the motor frequently starts [25,26].

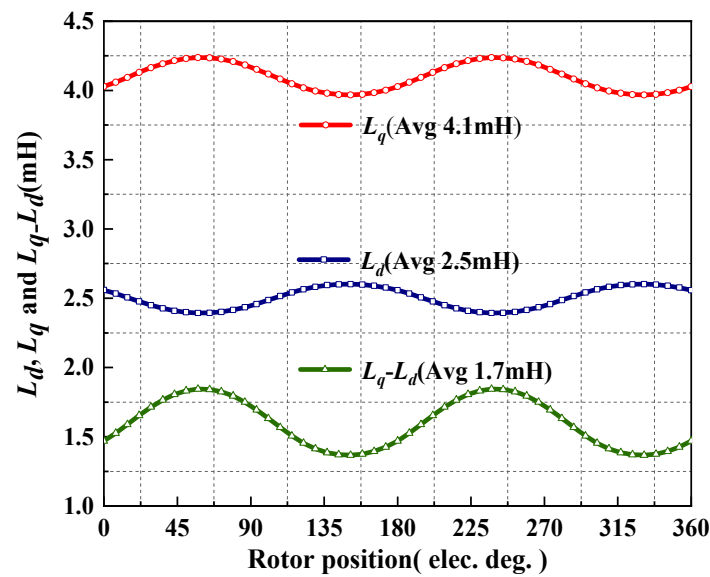


Figure 13. d-q axis inductances with rotor position.

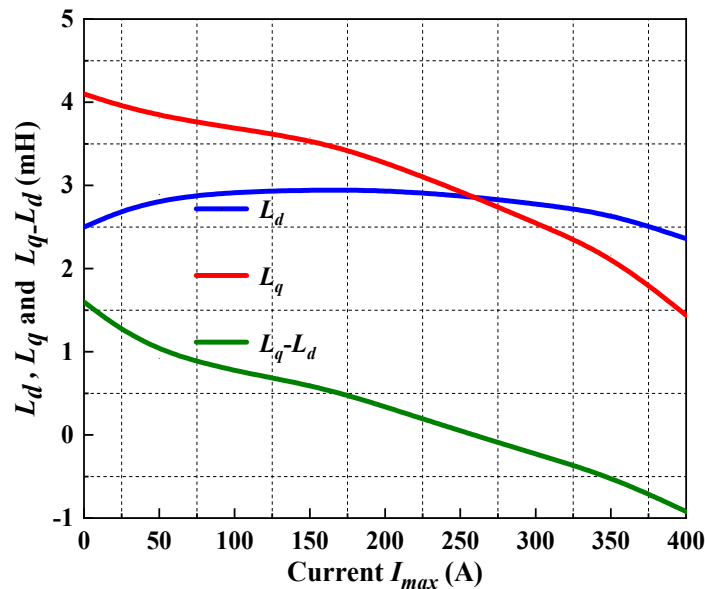


Figure 14. d-q inductances with the current  $I_{max}$ .

### 3. Mathematical Model of Modular Three-Phase PMSM

#### 3.1. Topology Winding Inductance Mathematical Model

A  $3^N$ th-order inductance matrix for the modular three-phase PMSM can be described as

$$L_{ij} = \begin{bmatrix} L_{AiAj} & L_{AiBj} & L_{AiCj} \\ L_{BiAj} & L_{BiBj} & L_{BiCj} \\ L_{CiAj} & L_{CiBj} & L_{CiCj} \end{bmatrix} \quad (3)$$

When  $i = j$ , the  $L_{ij}$  is the inductance matrix of  $i$ th motor unit, as expressed in the three-phase counterpart. When  $i \neq j$ , the mutual inductance matrix between each motor unit is negligible and can be ignored, which means  $L_{ij} = 0$ .

In the case of only considering the dc and second-harmonic component, the mathematical expressions of the inductances of each motor unit can be expressed as

$$\begin{cases} L_{AiAi} = L_{s0} + L_{s2} \cos(2\theta) \\ L_{BiBi} = L_{s0} + L_{s2} \cos 2(\theta - 2\pi/3) \\ L_{CiCi} = L_{s0} + L_{s2} \cos 2(\theta + 2\pi/3) \end{cases} \quad (4)$$

$i = 1, 2, 3$

$$\begin{cases} L_{BiCi} = L_{CiBi} = -L_{s00} + L_{s20} \cos(2\theta) \\ L_{BiAi} = L_{AiBi} = -L_{s00} + L_{s20} \cos 2(\theta - 2\pi/3) \\ L_{AiBi} = L_{BiAi} = -L_{s01} + L_{s21} \cos 2(\theta + 2\pi/3) \end{cases} \quad (5)$$

$i = 1, 2, 3$

where  $L_{s2}$  and  $L_{s0}$  are the 2nd harmonic and dc component of the self-inductances.  $L_{s00}$  and  $L_{s20}$  are the dc component and second-harmonic of the two adjacent phases of each motor unit (i.e., the phases A-C and B-C).  $L_{s01}$  and  $L_{s21}$  are the dc component and second-harmonic of the two alternate phases of each motor unit (i.e., the phase A-B).

### 3.2. Mathematical Equation of Modular Three-Phase PMSM

As mentioned above, the mutual inductances among the modular winding sets are negligible, enabling independent control. Thus, the proposed machine can be modeled as multiple segregated three-phase PMSMs, reducing the mathematical model complexity. Thus, the d-q axis model of the proposed machine in the synchronous rotor reference frame can be expressed by the traditional three-phase PMSM [14,20,21]. In this case, the d-q axis voltage transformation of each three-phase winding set can be expressed as

$$\begin{bmatrix} u_{dj} \\ u_{qj} \end{bmatrix} = \frac{2}{3} \begin{bmatrix} \cos \theta & \cos(\theta - \frac{2\pi}{3}) & \cos(\theta + \frac{2\pi}{3}) \\ -\sin \theta & -\sin(\theta - \frac{2\pi}{3}) & -\sin(\theta + \frac{2\pi}{3}) \end{bmatrix} \begin{bmatrix} u_{aj} \\ u_{bj} \\ u_{cj} \end{bmatrix} \quad (6)$$

where  $u_{aj}$ ,  $u_{bj}$ ,  $u_{cj}$  and  $u_{dj}$ - $u_{qj}$  represent the three-phase windings and d-q axis voltages of the  $j$ th motor unit. When the d-q transformation is applied to the proposed machine, the voltage and flux equation can be written as

$$\begin{bmatrix} u_{dj} \\ u_{qj} \end{bmatrix} = R \begin{bmatrix} i_{dj} \\ i_{qj} \end{bmatrix} + \frac{d}{dt} \begin{bmatrix} \psi_{dj} \\ \psi_{qj} \end{bmatrix} + \omega_e \begin{bmatrix} -\psi_{qj} \\ \psi_{dj} \end{bmatrix} \quad (7)$$

$$\begin{bmatrix} \psi_{dj} \\ \psi_{qj} \end{bmatrix} = \begin{bmatrix} L_d & 0 \\ 0 & L_q \end{bmatrix} \begin{bmatrix} i_{dj} \\ i_{qj} \end{bmatrix} + \psi_r \begin{bmatrix} 1 \\ 0 \end{bmatrix} \quad (8)$$

where  $i_{dj}$  and  $i_{qj}$  are the d-q axis currents,  $R$  is the stator resistance,  $L_d$  and  $L_q$  are the d-q axis inductance,  $\omega_e$  is the electric angular velocity, and  $\psi_r$  is the PM flux linkage. By substituting (8) into (7), the following equations are easy to obtain:

$$\begin{cases} \frac{di_{dj}}{dt} = -\frac{R}{L_d} i_{dj} + \frac{L_q}{L_d} \omega_e i_{qj} + \frac{1}{L_d} u_{dj} \\ \frac{di_{qj}}{dt} = -\frac{R}{L_q} i_{qj} - \frac{L_d}{L_q} \omega_e i_{dj} - \frac{\psi_r}{L_q} \omega_e + \frac{1}{L_q} u_{qj} \end{cases} \quad (9)$$

As is stated above, the torque generated by the proposed machine will be the algebraic sum of the torque generated by each three-phase motor unit sharing the common rotor. Thus, the resultant electromagnetic torque equation of the modular three-phase PMSM can be written as

$$T_e = \frac{3n_p}{2} \sum_{j=1}^N (\psi_r i_{qj} + (L_d - L_q) i_{dj} i_{qj}) \tag{10}$$

Similarly, the mechanical dynamic model of the proposed machine can be written as

$$T_e - T_L = \frac{J}{n_p} \frac{d\omega_e}{dt} \tag{11}$$

where  $n_p$  is the pole of pairs,  $J$  is the moment of inertia,  $T_e$  is the electromagnetic torque, and  $T_L$  is the load torque.

#### 4. PTC of Modular Three-Phase PMSM

Taking the six-module three-phase PMSM as an example, as shown in Figure 15, the six stator winding coils of the six-module three-phase PMSM are connected to six VSIs in parallel. Each three-phase winding set is fed independently by a VSI. The behavior of each set of VSIs is identical with the traditional three-phase counterpart, and the behaviors of the six VSIs are identical. Therefore, the control of a VSI can realize the operation of the six-module three-phase PMSM. The control block diagram of the six-module three-phase PMSM system with the PTC method is described in Figure 15a. The stator flux and torque prediction control unit are based on Equations (13)–(16). Then, the detected d-q axis current is input to the state flux and torque prediction control unit. The predicted values of the torque and flux of the machine are input the cost function. The cost function is based on the algorithm proposed in this paper to send out the PWM modulation signal to realize the control of the module three-phase PMSM. Besides, the six-module three-phase PMSM system with the double closed-loop vector control system, which adopts the maximum torque current per ampere (MPTA), is shown in Figure 15b.

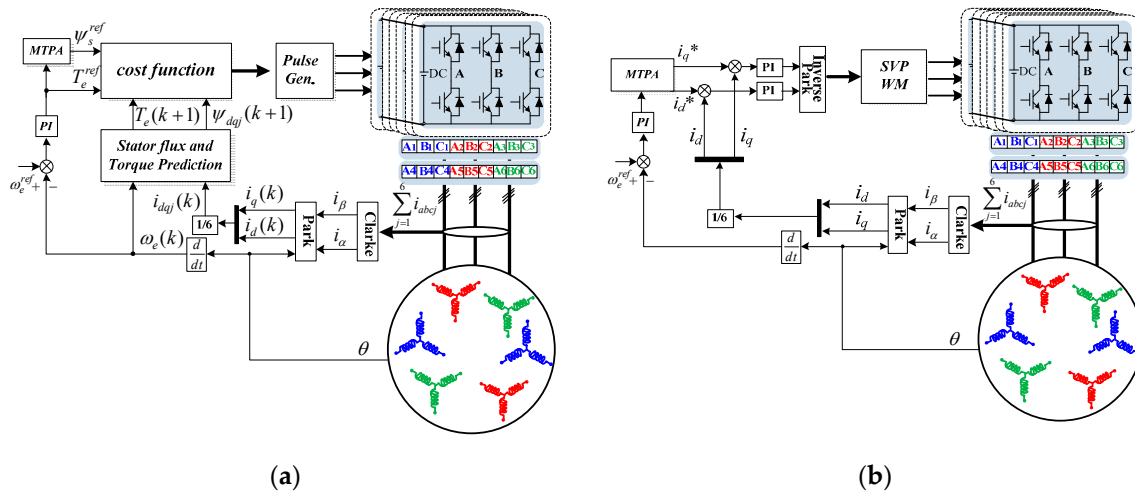


**Figure 15.** Structural diagram of the six modular three-phase PMSM: (a) with the predictive torque control (PTC) method, (b) with the proportional-integral (PI).

To realize the predicted stator flux and the predicted torque track their reference values accurately, the cost function can be given by

$$g = k_\psi \left| \psi_s^{ref} - \psi_s(k+1) \right| + \left| T_e^{ref} - T_e(k+1) \right| \tag{12}$$

where  $T_e^{ref}$  is the torque reference and the  $\psi_s^{ref}$  is the flux linkage reference;  $T_e(k+1)$  is the predicted torque,  $\psi_s(k+1)$  is the predicted flux linkage; and  $k_\psi$  is a weighting factor.

The  $T_s$  is the sampling period and is short enough. The prediction equation of torque and stator flux of the proposed machine can be expressed as

$$\begin{cases} \psi_s(k+1) = \sqrt{\psi_{d_j}^2(k+1) + \psi_{q_j}^2(k+1)} \\ T_e(k+1) = \frac{3n_p}{2} \sum_{j=1}^N [\psi_r i_{q_j}(k+1) + (L_d - L_q) i_{d_j}(k+1) i_{q_j}(k+1)] \end{cases} \quad (13)$$

where  $\psi_{d_j}(k+1)$  and  $\psi_{q_j}(k+1)$  are the  $d$ - $q$  axis predicted stator flux linkage value; and  $i_{d_j}(k+1)$  and  $i_{q_j}(k+1)$  are the  $d$ -axis and  $q$ -axis predicted current value.

According to (9), the discrete state equation of the modular three-phase PMSM can be expressed as

$$\begin{cases} i_{d_j}(k+1) = \frac{1}{L_d} T_s u_{d_j}(k) - (\frac{R}{L_d} T_s - 1) i_{d_j}(k) + \frac{L_q}{L_d} T_s \omega_e(k) i_{q_j}(k) \\ i_{q_j}(k+1) = \frac{1}{L_q} T_s u_{q_j}(k) - (\frac{R}{L_q} T_s - 1) i_{q_j}(k) - \frac{L_d}{L_q} T_s \omega_e(k) i_{d_j}(k) - \frac{1}{L_q} T_s \psi_r \omega_e(k) \end{cases} \quad (14)$$

where  $u_{d_j}(k+1)$  and  $u_{q_j}(k+1)$  are the  $d$ - $q$  axis predicted stator voltage. According to (14), the stator flux prediction equation of the modular three-phase PMSM can be obtained as

$$\begin{cases} \psi_{d_j}(k+1) = T_s u_{d_j}(k) + (1 - \frac{R}{L_d} T_s) \psi_{d_j}(k) + T_s \omega_e(k) \psi_{q_j}(k) + \frac{R}{L_d} \psi_r T_s \\ \psi_{q_j}(k+1) = T_s u_{q_j}(k) + (1 - \frac{R}{L_q} T_s) \psi_{q_j}(k) - T_s \omega_e(k) \psi_{d_j}(k) \end{cases} \quad (15)$$

The relationship between stator flux and torque reference can be estimated with the MPTA control strategy [23,24].

$$\psi_s^{ref} = \sqrt{\psi_d^2 + \psi_q^2} = \sqrt{(\psi_r)^2 + (L_q \cdot \frac{T_e^{ref}}{\frac{3Nn_p}{2} \psi_r})^2} \quad (16)$$

Taking the six-module three-phase PMSM as an example, the control system simulation model is built up using the MATLAB/Simulink, as shown in Figure 16. There is no original mathematical model of the prototype in Matlab/Simulink, so the mathematical model of the proposed machine must be built to verify the effectiveness and control algorithm. The six-module three-phase PMSM model is built based on the Equations (7)–(11), and the model of the controller is established by Equations (12)–(16). The overall control block diagram and the mathematical model of a motor established in Matlab/Simulink are shown in Figure 16. The validity of the proposed control approach is verified by the simulation analysis results. The main parameters of the unit motor used in the MATLAB/Simulink are listed in Table 3. The 5000 is the weight factor of the control approach, the sampling frequency is set to 10 kHz, and the IGBT switching frequency is 5 kHz. The proportion coefficient and integral coefficient of the PI speed controller are 8000 and 0.5, respectively. When the PI control strategy is adopted, the proportion coefficient and integral coefficient of the PI double current loop are 0.26 and 65.7. At this time, the output torque ripple of the proposed machine is minimum.

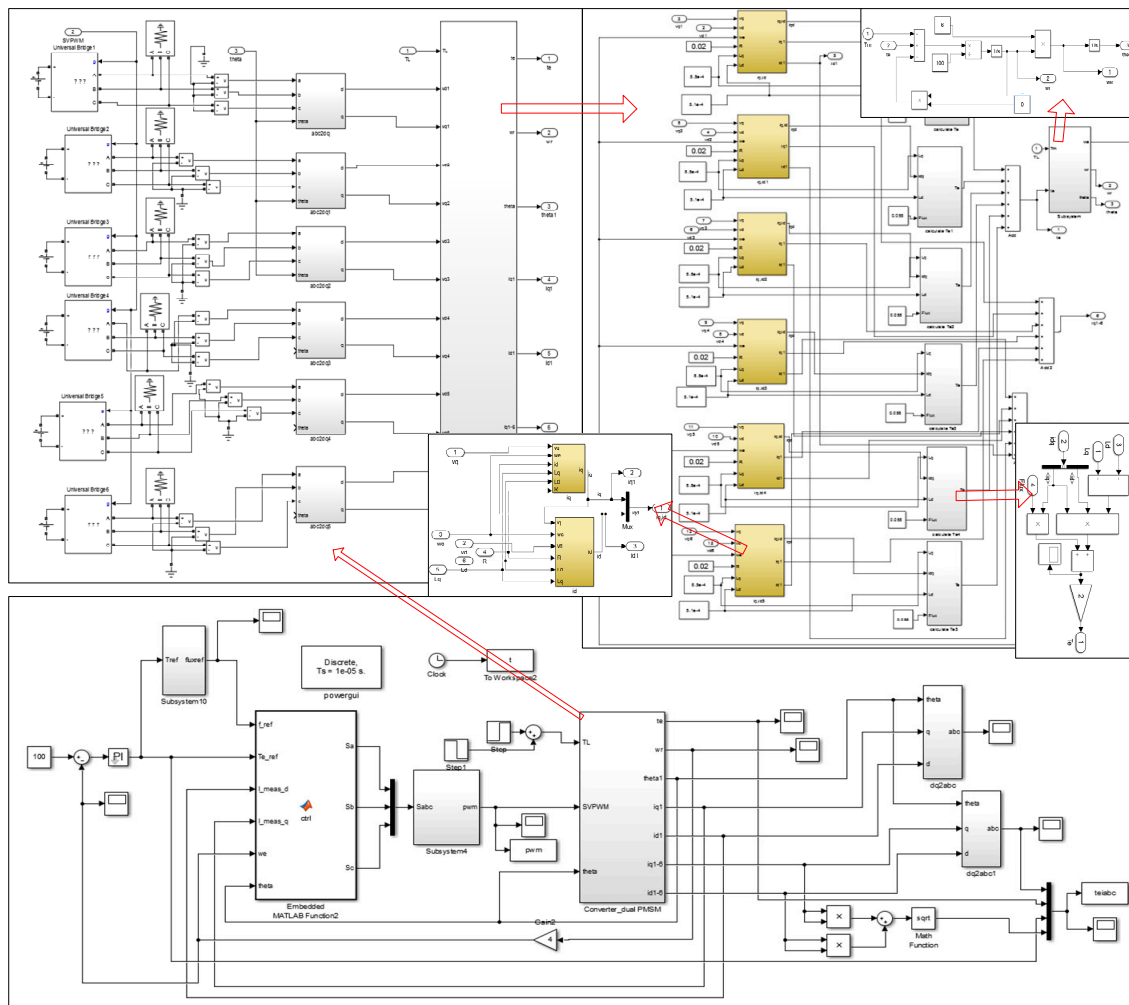


Figure 16. The Matlab/Simulink model of the modular machine and of the control system.

Table 3. Main Parameters of Three-phase permanent magnet synchronous motor (PMSM) unit.

Parameter	Value	Parameter	Value
Rated power	20 kW	Rotor flux	0.058 Wb
Rated voltage	380 V	Stator resistance	0.07 Ω
Rated speed	600 r/min	d inductance	0.51 mH
DC bus voltage	250 V	q inductance	0.85 mH
Pole pairs	2	-	-

### 5. Experimental Results and Analysis

The control performances of the six-module three-phase PMSM by using the proposed PTC method are depicted in Figures 17–19. At 0 s, the speed and torque reference are respectively set as 600 rpm and 8000 Nm. At 0.35 s, the load torque of the six-module three-phase PMSM suddenly steps to 1000 Nm. The load torque steps to 1600 Nm at 0.8 s, then back to 1000 Nm at 1.2 s. The simulation analysis results of the torque and phase current of the six-module three-phase PMSM are depicted in Figure 17. The Figure 17a shows the PTC control algorithm proposed in this paper can well follow the change of load torque. It is seen that the peak-to-peak torque ripple of the six-module three-phase PMSM is about ±200 Nm and the peak-to-peak torque ripple with the PI controller is about ±300 Nm, as shown in Figure 17b, which means the torque ripple mainly caused by the asymmetrical mutual inductances can be dramatically reduced by using the proposed PTC method. The simulation analysis results of the  $\alpha$ - $\beta$  stator flux linkage of the six-module three-phase PMSM is depicted in Figure 18.

It shows that the predicted value of the  $\alpha$ - $\beta$  stator flux linkage can accurately track the reference value. The tracking error of  $\alpha$ - $\beta$  stator flux linkage are  $\pm 0.01$  Wb, and the fluctuation range of the  $\alpha$ - $\beta$  stator flux linkage is from 0.8 Wb to 0.83 Wb. The simulation results of the three-dimensional rotor flux trajectories of the six-module three-phase PMSM, as shown in Figure 19. It shows a small  $\alpha$ - $\beta$  stator flux linkage track error between the predicted flux linkage and the reference value.

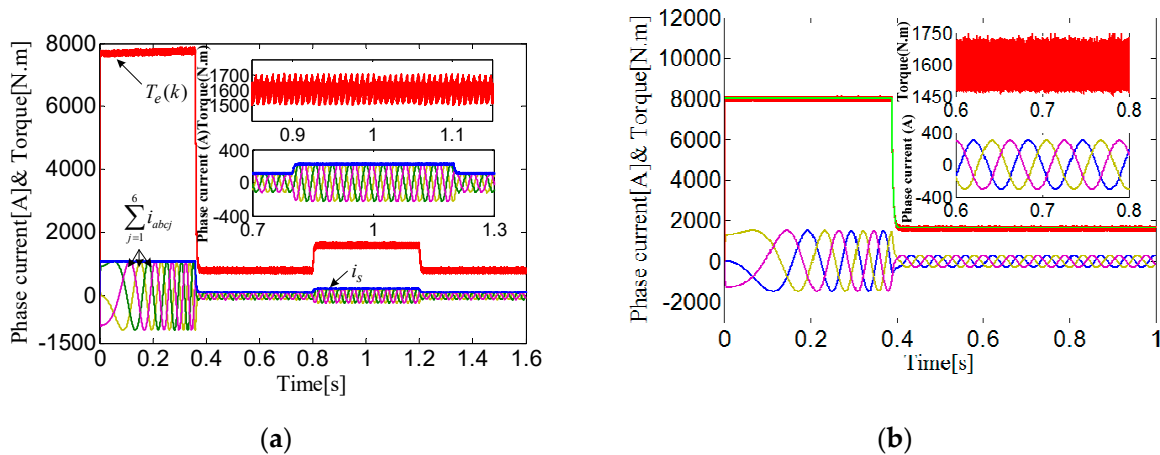


Figure 17. The current and torque: (a) with proposed PTC, (b) with PI.

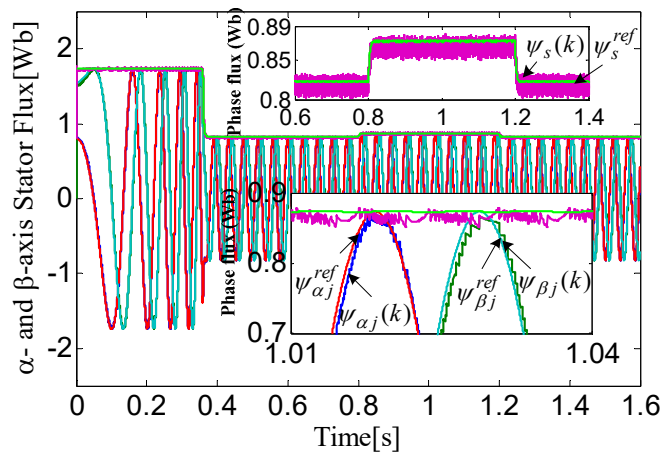


Figure 18.  $\alpha$ - $\beta$  stator flux linkage.

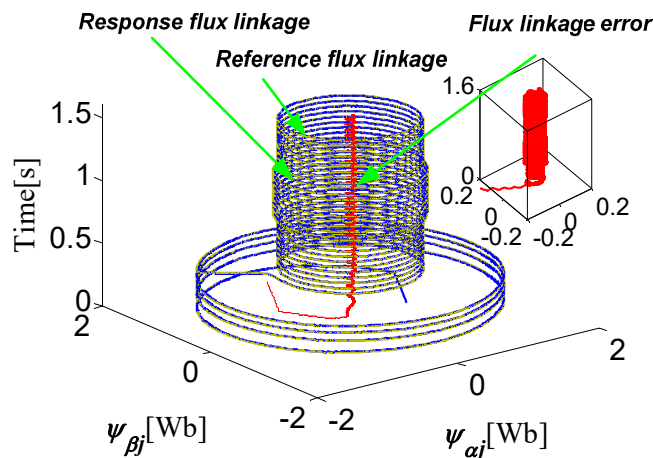


Figure 19. Three-dimensional view of the rotor flux trajectories.

Figure 20 presents the frequency spectra of the stator current of the unit motor of the six-module three-phase PMSM and unit motor. It is seen from Figure 20 that the fundamental value of the unit motor is 74.44 A. The THD of the unit motor of the six-module three-phase PMSM is 2.82%. The above simulation analysis shows that the six module three-phase PMSM can achieve perfect control performance and lower harmonic content with the proposed PTC method.

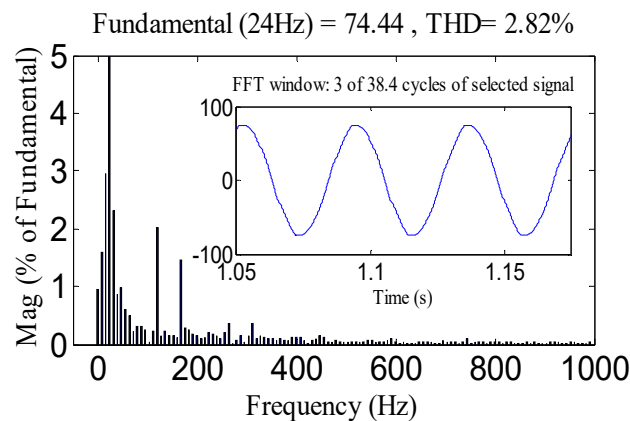


Figure 20. The frequency spectra of stator current  $i_a$  at 1600 Nm of the motor unit.

Furthermore, in order to further verify the feasibility of the proposed control method of the six-module three-phase PMSM, a test prototype was made, as shown in Figure 21. Each unit motor had 4 poles and 24 slots. In order to further reduce the magnetic coupling between each unit motor, magnetic isolation material was used between each unit motor. The main parameters of the unit motor are listed in Table 3, and an experimental platform was set up and described in Figure 22. It mainly included: one six-module three-phase PMSM, A DC load motor, a load motor control cabinet, 6 integrated power module-based converters, a real-time monitoring display, and so on. The DSP28335 was selected as the main control chip, the torque sensor was HBM T20WN, and the current sensor was Tek A622 current clamp.

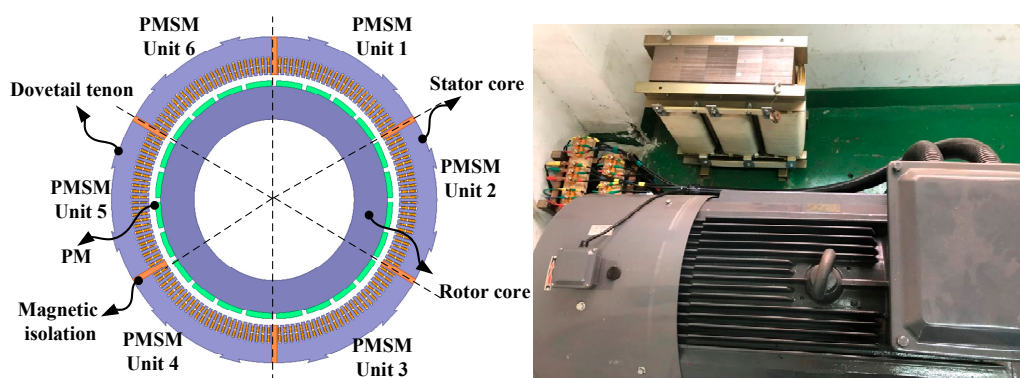


Figure 21. Schematic diagram of the prototype structure and the physical drawing of the prototype.



Figure 22. 6\*three-phase PMSM experimental platform.

High-frequency voltage impulse method was used to obtain the values of d-q axis inductances of the prototype. The Figure 23 is the inductance waveform of the dq axis tested in practice. In the case of the rated load, the measured  $L_d$  (0.38 mH) is smaller than the  $L_d$  (0.51 mH) obtained by FEA, and the measured  $L_q$  (0.91 mH) is bigger than the  $L_q$  (0.85 mH) obtained by FEA.

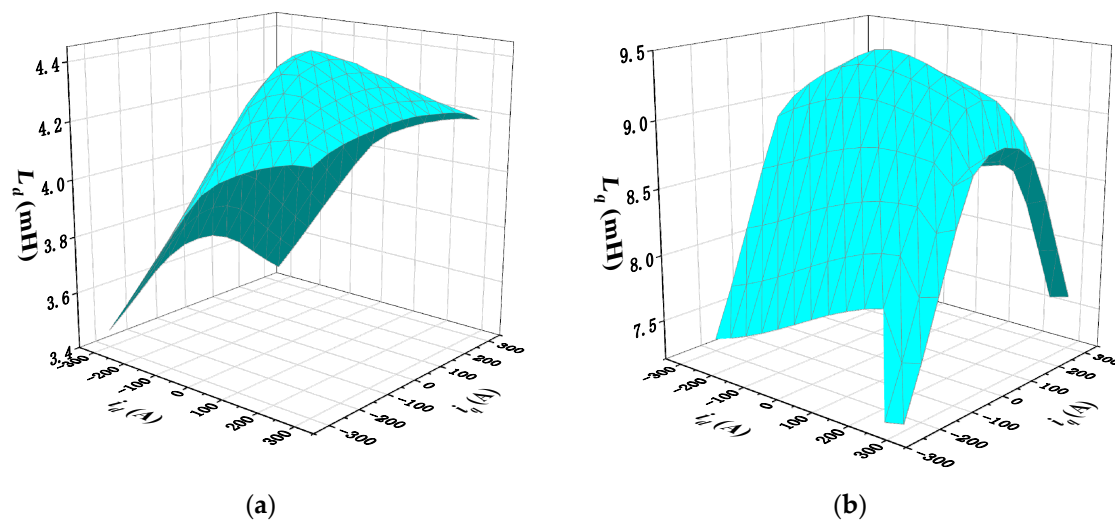


Figure 23. Measured dq axis inductance: (a)  $L_d$ , (b)  $L_q$ .

Figure 24a shows the experimental results of the phase current and torque of the unit motor. The experimental analysis results of the phase current and torque of the unit motor of six-module three-phase PMSM are given in Figure 24a. The experimental results show that the unit motor can achieve an excellent stator current and work well in dynamic conditions, in terms of load torque changes. The response speed of the system is very fast by using the proposed PTC method. The experimental analysis results of the  $\alpha$ - $\beta$  stator flux linkage of the unit motor of six-module three-phase PMSM are illustrated in Figure 24b. The predicted flux linkage value of the unit motor of six module three-phase PMSM can accurately track its reference value, which is shown in Figure 24b. Figure 25 shows the current waveforms of the unit motor with the PTC method in the paper. According to the test results, the THD of the six-module three-phase PMSM with the PTC method proposed in the paper is 3.1% with low harmonic content.

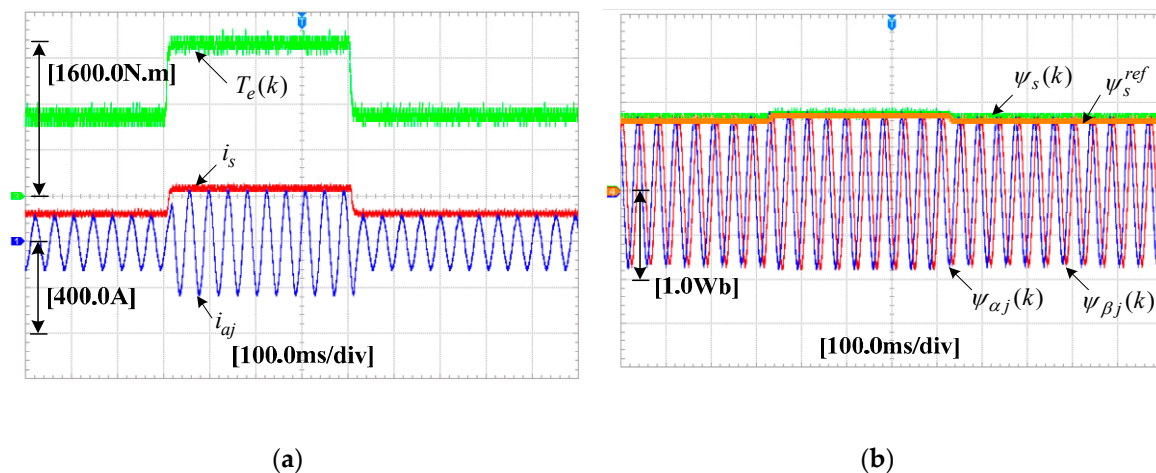


Figure 24. Experimental results: (a) current and torque, (b)  $\alpha$ - $\beta$  stator flux linkage.

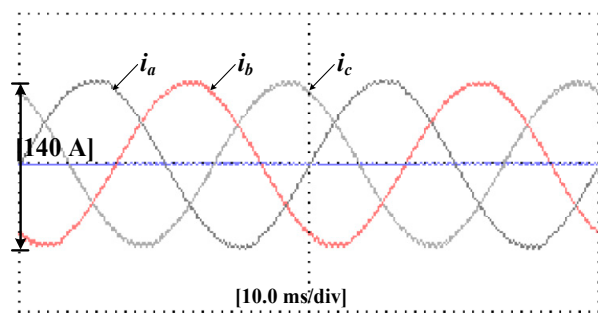


Figure 25. Current waveform with proposed PTC method.

## 6. Conclusions

In view of the disadvantages of conventional multi-three-phase PMSM drive systems, such as complex structure, custom, and expensive converters, a novel modular three-phase PMSM with PTC method control strategy has been proposed in this paper. This novel machine is composed of  $N$  sets of three-phase PMSM units with the same electromagnetic characteristics. Each motor unit has the advantages of good electrical/magnetic isolation, simple structure, and easy control. The study also found that the salient effect will exist in each motor unit caused by the inconsistent mutual inductances of three phase windings, even if the machine adopts the surface-mounted PM rotor structure. This feature is distinctive and unavoidable for the machine with the segregated winding configuration and should be considered in establishing accurate mathematical modeling for modular three-phase PMSM. Moreover, the simulation results show that the torque ripple achieved is lower than that obtained with the PI method, and the experimental results show that a small current THD can be achieved.

**Author Contributions:** Conceived the theory and built the model, Z.R.; performed the simulations and experiments and analyzed the data, W.Z. and G.W.; wrote the paper, Z.R. and J.Z.; funding acquisition, S.H. All authors have read and agreed to the published version of the manuscript.

**Funding:** This work was supported in part the State Key Program of National Natural Science of China (Grant number 51737004).

**Conflicts of Interest:** The authors declare no conflict of interest.

## References

1. Hu, F.; Luo, D.; Luo, C.; Long, Z.; Wu, G. Cascaded Robust Fault-Tolerant Predictive Control for PMSM Drives. *Energies* **2018**, *11*, 3087. [[CrossRef](#)]
2. Wang, K.; Lin, H. Modular Permanent Magnet Synchronous Machine with Low Space Harmonic Content. *Energies* **2020**, *13*, 3924. [[CrossRef](#)]
3. Welchko, B.; Nagashima, J. The influence of topology selection on the design of EV/HEV propulsion systems. *IEEE Power Electron. Lett.* **2003**, *2*, 36–40. [[CrossRef](#)]
4. Jung, E.; Yoo, H.; Sul, S.-K.; Choi, H.-S.; Choi, Y.-Y. A Nine-Phase Permanent-Magnet Motor Drive System for an Ultrahigh-Speed Elevator. *IEEE Trans. Ind. Appl.* **2012**, *48*, 987–995. [[CrossRef](#)]
5. Takorabet, V.N.; Caron, J.P.; Mobarakeh, B.N.; Tabar, F.M.; Humbert, G. Study of different architectures of fault-tolerant actuator using a two-channel PM motor. *IEEE Trans. Ind. Appl.* **2011**, *47*, 47–54.
6. Patel, V.I.; Wang, J.; Nair, S.S. Demagnetization Assessment of Fractional-Slot and Distributed Wound 6-Phase Permanent Magnet Machines. *IEEE Trans. Magn.* **2015**, *51*, 1–11. [[CrossRef](#)]
7. Miyama, Y.; Akatsu, K. Technical arrangement of high-performance techniques achieved by multi-phase permanent magnet synchronous motor systems. In Proceedings of the Energy Conversion Congress and Exposition, Portland, USA, 23–27 September 2018; pp. 1574–1580. [[CrossRef](#)]
8. Wang, X.; Wang, Z.; Xu, Z. A Hybrid Direct Torque Control Scheme for Dual Three-Phase PMSM Drives with Improved Operation Performance. *IEEE Trans. Power Electron.* **2018**, *34*, 1622–1634. [[CrossRef](#)]
9. Cui, S.; Zhao, T.; Du, B.; Cheng, Y. Multiphase PMSM with Asymmetric Windings for Electric Drive. *Energies* **2020**, *13*, 3765. [[CrossRef](#)]
10. Abdullah, A.A.; Dordevic, O.; Jones, M.; Levi, E. Regenerative Test for Multiple Three-Phase Machines With Even Number of Neutral Points. *IEEE Trans. Ind. Electron.* **2020**, *67*, 1684–1694. [[CrossRef](#)]
11. Lamichhane, A.; Zhou, L.; Yao, G.; Luqman, M. Modeling, Control and Power Management of Six-Phase PMSM Based Shipboard MVDC Distribution System. *Energies* **2020**, *13*, 4229. [[CrossRef](#)]
12. Demir, Y.; Yolacan, E.; El-Refaie, A.M.; Aydin, M. Investigation of Different Winding Configurations and Displacements of a Nine-Phase Permanent-Magnet-Synchronous Motor With Unbalanced AC Winding Structure. *IEEE Trans. Magn.* **2019**, *55*, 3660–3670. [[CrossRef](#)]
13. Demir, Y.; Aydin, M. A Novel Asymmetric and Unconventional Stator Winding Configuration and Placement for a Dual Three-Phase Surface PM Motor. *IEEE Trans. Magn.* **2017**, *53*, 1–5. [[CrossRef](#)]
14. Önsal, M.; Demir, Y.; Aydin, M. A New Nine-Phase Permanent Magnet Synchronous Motor With Consequent Pole Rotor for High-Power Traction Applications. *IEEE Trans. Magn.* **2017**, *53*, 1–6. [[CrossRef](#)]
15. Demir, Y.; Aydin, M. A Novel Dual Three-Phase Permanent Magnet Synchronous Motor With Asymmetric Stator Winding. *IEEE Trans. Magn.* **2016**, *52*, 1–5. [[CrossRef](#)]
16. Barcaro, M.; Bianchi, N.; Magnussen, F. Analysis and Tests of a Dual Three-Phase 12-Slot 10-Pole Permanent-Magnet Motor. *IEEE Trans. Ind. Appl.* **2010**, *46*, 2355–2362. [[CrossRef](#)]
17. Luise, F.; Pieri, S.; Mezzarobba, M.; Tassarolo, A. Regenerative Testing of a Concentrated-Winding Permanent-Magnet Synchronous Machine for Offshore Wind Generation—Part I: Test Concept and Analysis. *IEEE Trans. Ind. Appl.* **2012**, *48*, 1779–1790. [[CrossRef](#)]
18. Luise, F.; Pieri, S.; Mezzarobba, M.; Tassarolo, A. Regenerative Testing of a Concentrated-Winding Permanent-Magnet Synchronous Machine for Offshore Wind Generation—Part II: Test Implementation and Results. *IEEE Trans. Ind. Appl.* **2012**, *48*, 1791–1796. [[CrossRef](#)]
19. Wang, B.; Wang, J.; Griffo, A.; Sen, B. A general modeling technique for a triple redundant  $3 \times 3$ -phase PMA SynRM. *IEEE Trans. Ind. Electron.* **2018**, *65*, 9068–9078. [[CrossRef](#)]
20. Han, X.; Jiang, D.; Zou, T.; Qu, R.; Yang, K. Two-Segment Three-Phase PMSM Drive With Carrier Phase-Shift PWM for Torque Ripple and Vibration Reduction. *IEEE Trans. Power Electron.* **2019**, *34*, 588–599. [[CrossRef](#)]
21. Bhattacharya, S.; Mascarella, D.; Joos, G.; Cyr, J.-M.; Xu, J. A Dual Three-Level T-NPC Inverter for High-Power Traction Applications. *IEEE J. Emerg. Sel. Top. Power Electron.* **2016**, *4*, 668–678. [[CrossRef](#)]
22. Belda, K.; Vosmik, D. Explicit Generalized Predictive Control of Speed and Position of PMSM Drives. *IEEE Trans. Ind. Electron.* **2016**, *6*, 3889–3896. [[CrossRef](#)]
23. Zhang, C.; Wu, G.; Rong, F.; Feng, J.; Jia, L.; He, J.; Huang, S.; Fei, R. Robust Fault-Tolerant Predictive Current Control for Permanent Magnet Synchronous Motors Considering Demagnetization Fault. *IEEE Trans. Ind. Electron.* **2017**, *65*, 5324–5534. [[CrossRef](#)]

24. Huang, S.; Wu, G.; Rong, F.; Zhang, C.; Huang, S.; Wu, Q. Novel predictive stator flux control techniques for PMSM drives. *IEEE Trans. Power Electron.* **2018**, *34*, 8916–8929. [[CrossRef](#)]
25. Zhu, X.; Wu, W.; Yang, S.; Xiang, Z.; Quan, L. Comparative Design and Analysis of New Type of Flux-Intensifying Interior Permanent Magnet Motors With Different Q-Axis Rotor Flux Barriers. *IEEE Trans. Energy Convers.* **2018**, *33*, 2260–2270. [[CrossRef](#)]
26. Zhu, X.; Huang, J.; Quan, L.; Xiang, Z.; Shi, B. Comprehensive Sensitivity Analysis and Multiobjective Optimization Research of Permanent Magnet Flux-Intensifying Motors. *IEEE Trans. Ind. Electron.* **2019**, *66*, 2613–2627. [[CrossRef](#)]

**Publisher’s Note:** MDPI stays neutral with regard to jurisdictional claims in published maps and institutional affiliations.



© 2020 by the authors. Licensee MDPI, Basel, Switzerland. This article is an open access article distributed under the terms and conditions of the Creative Commons Attribution (CC BY) license (<http://creativecommons.org/licenses/by/4.0/>).